Photoelectrochemistry

International Edition: DOI: 10.1002/anie.201805027
German Edition: DOI: 10.1002/ange.201805027

# Solar Water Splitting with a Hydrogenase Integrated in Photoelectrochemical Tandem Cells

*Dong Heon Nam, Jenny Z. Zhang, Virgil Andrei, Nikolay Kornienko, Nina Heidary, Andreas Wagner, Kenichi Nakanishi, Katarzyna P. Sokol, Barnaby Slater, Ingo Zebger, Stephan Hofmann, Juan C. Fontecilla-Camps, Chan Beum Park, and Erwin Reisner**

***Abstract:*** *Hydrogenases ($H_2$ases) are benchmark electrocatalysts for $H_2$ production, both in biology and (photo)catalysis in vitro. We report the tailoring of a p-type Si photocathode for optimal loading and wiring of $H_2$ase through the introduction of a hierarchical inverse opal (IO) $TiO_2$ interlayer. This proton-reducing Si | IO-$TiO_2$ | $H_2$ase photocathode is capable of driving overall water splitting in combination with a photoanode. We demonstrate unassisted (bias-free) water splitting by wiring Si | IO-$TiO_2$ | $H_2$ase to a modified $BiVO_4$ photoanode in a photoelectrochemical (PEC) cell during several hours of irradiation. Connecting the Si | IO-$TiO_2$ | $H_2$ase to a photosystem II (PSII) photoanode provides proof of concept for an engineered Z-scheme that replaces the non-complementary, natural light absorber photosystem I with a complementary abiotic silicon photocathode.*

The capture and storage of solar energy in the form of $H_2$ through water splitting is a promising process to produce sustainable fuel. Hydrogenases ($H_2$ases) are metalloenzymes that operate at the thermodynamic potential for proton reduction, which makes them attractive noble-metal-free model catalysts.[1] $H_2$ases have been combined with a series of light absorbers, such as dye-sensitized $TiO_2$, carbon nitrides, cadmium-based and carbon nanodots, $In_2S_3$ nanoparticles, and organic dyes, for photocatalytic $H_2$ production in the presence of a sacrificial electron donor.[2] Sacrificial reagents can be avoided by using a photoelectrochemistry (PEC) approach with $H_2$ases wired to electrodes, but these systems have relied on an external applied voltage to drive water splitting into $H_2$ and $O_2$.[3] Thus unassisted solar water splitting with a $H_2$ase in vitro has been a long-standing goal.

Silicon (Si) has a narrow band gap of 1.1 eV and is widely used as an efficient photocathode for proton reduction. Its use requires protection of the Si surface from the aqueous electrolyte solution (typically with a $TiO_2$ coating) and modification with a $H_2$ evolution catalyst.[4] Previous reports on p-Si photocathodes modified with $H_2$ase suffered from low photocurrents or Faradaic efficiencies, which can be attributed to a small effective surface area of the electrode and suboptimal integration of the $H_2$ase into the materials architecture.[3c,5]

Herein, we report the assembly of a Si-based photoelectrode that features a hierarchically structured inverse opal (IO)-$TiO_2$ layer optimized for high and stable integration of a [NiFeSe]-$H_2$ase from *Desulfomicrobium baculatum* as the $H_2$ evolution biocatalyst.[1b,6] The Si | IO-$TiO_2$ | $H_2$ase photocathode can be coupled to complementary photoanodes for water oxidation to achieve overall water splitting (see the Supporting Information, Figure S1). We investigated coupling of the Si | IO-$TiO_2$ | $H_2$ase to an abiotic (n-type $BiVO_4$) and a biotic (Photosystem II, PSII) photoanodic system for overall water splitting.

A 4 nm thick $TiO_2$ layer was deposited on the surface of a p-Si wafer by atomic layer deposition (ALD) immediately after hydrofluoric acid (HF) treatment to protect the electrode from the formation of an insulating silica layer (Figures S2 and S3). A hierarchically structured IO-$TiO_2$ layer of 10 μm film thickness was subsequently assembled on top of the ALD layer by co-assembly of $TiO_2$ nanoparticles (P25, 21 nm) with polystyrene beads (750 nm), followed by heating at 450 °C.[3a] Characterization by scanning electron microscopy (SEM; Figures 1 A and S4) showed a macropore diameter of 750 nm, facilitating the penetration of large biomolecules. X-ray diffraction (XRD) and UV/Vis spectroscopy confirmed the expected crystallinity and transparency in the visible spectrum for IO-$TiO_2$ (Figure S5).

[*] Dr. D. H. Nam, Dr. J. Z. Zhang, V. Andrei, Dr. N. Kornienko, Dr. N. Heidary, A. Wagner, K. P. Sokol, B. Slater, Prof. E. Reisner
Department of Chemistry, University of Cambridge
Cambridge CB2 1EW (UK)
E-mail: reisner@ch.cam.ac.uk
Homepage: http://www-reisner.ch.cam.ac.uk/

K. Nakanishi, Prof. S. Hofmann
Department of Engineering, University of Cambridge
Cambridge CB3 0FA (UK)

Dr. I. Zebger
Max Volmer Laboratorium für Biophysikalische Chemie, Sekretariat PC14, Institut für Chemie, Technische Universität Berlin
Straße des 17. Juni 135, 10623 Berlin (Germany)

Dr. J. C. Fontecilla-Camps
Metalloproteins Unit, Institut de Biologie Structurale
Université Grenoble Alpes, CEA, CNRS, 38044 Grenoble (France)

Prof. C. B. Park
Department of Materials Science and Engineering
Korea Advanced Institute of Science and Technology
291 Daehak-ro, Yuseong-gu, Daejeon 34141 (Republic of Korea)

Supporting information and the ORCID identification number(s) for the author(s) of this article can be found under: https://doi.org/10.1002/anie.201805027. Additional data related to this publication are available at the University of Cambridge data repository: https://doi.org/10.17863/CAM.23972.

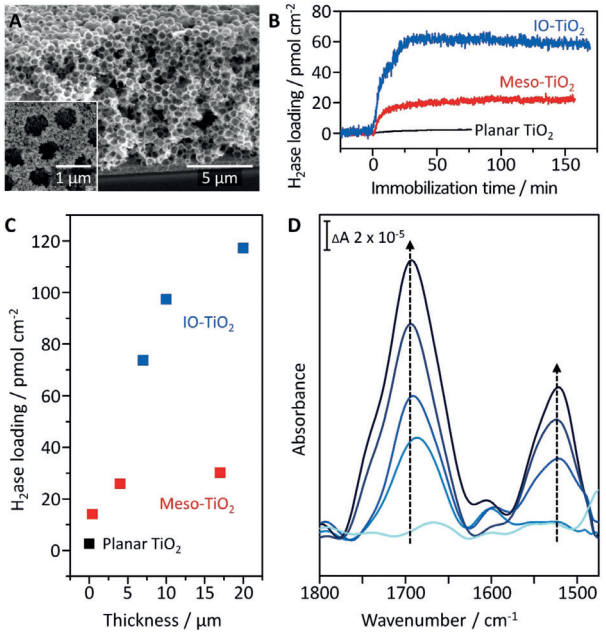


***Figure 1.*** A) Cross-sectional SEM image of the Si | IO-$TiO_2$ photocathode. Inset: Top-view SEM. B) Loading capacities and stabilities of immobilized $H_2$ase on planar, mesoporous (4 µm), and IO-$TiO_2$ (7 µm) electrodes studied by QCM analysis. C) QCM quantification of the $H_2$ase loading on different $TiO_2$ architectures with various film thicknesses. D) ATR-IR spectra of Si prism | IO-$TiO_2$ | $H_2$ase during incubation with $H_2$ase (10 µL of 8 µM) after 0, 7.5, 15, 22.5, and 30 min. The intensities of the amide I (1690 $cm^{-1}$) and II (1520 $cm^{-1}$) bands from the protein backbone of the $H_2$ase molecules increased with time in direction of the arrows. The penetration depth of the evanescent wave into the bottom of the 10 µm thick IO-$TiO_2$ from the ATR-Si prism surface is approximately 0.5 µm.

The ability of IO-$TiO_2$ to support high protein loadings was studied by quartz crystal microbalance (QCM) analysis. The IO-$TiO_2$ electrode at 7 µm thickness exhibited a 3 and 27 times higher loading capacity for $H_2$ase than mesoporous (>4 µm thickness; Figure S6) and planar $TiO_2$ electrodes, respectively (Figure 1B). The protein remained almost quantitatively adsorbed on the porous $TiO_2$ layers for more than two hours during the QCM measurement. The loading capacity of $H_2$ase increased with the film thickness of the IO-$TiO_2$ layer, whereas the loading on the mesoporous $TiO_2$ film saturated at a thickness of 4 µm (Figures 1C and S6).

Penetration of the $H_2$ase through the IO-$TiO_2$ architecture was then probed by attenuated total reflection infrared (ATR-IR) spectroscopy using a Si prism coated with an IO-$TiO_2$ layer (10 µm thickness). After addition of $H_2$ase (10 µL of 8 µM) to the buffer solution covering the IO-$TiO_2$ coated prism, two characteristic bands at 1690 $cm^{-1}$ and 1520 $cm^{-1}$, known as amide I (preferentially CO stretching) and amide II (mainly a combination of NH bending and CN stretching vibrations), were detected (Figure 1D).[7] The protein adsorption was monitored in situ and was still increasing after 30 min of incubation time. In this experimental setup, the penetration depth of the evanescent wave of the IR beam was restricted to approximately 0.5 µm from the Si prism surface, and the amide bands were therefore assigned to $H_2$ase that had infiltrated the entire IO-$TiO_2$ layer. For comparison, ATR-IR spectra of 1 µm thick mesoporous $TiO_2$ on a Si prism exhibited no amide bands even after incubation with $H_2$ase for 45 min (Figure S7). The hierarchical electrode structure has therefore been established as a superior scaffold for enzyme integration compared to meso- and flat $TiO_2$.[5] Thus, this Si | IO-$TiO_2$ | $H_2$ase was employed in all PEC experiments.

Drop-casting of $H_2$ase (80 pmol) onto the IO-$TiO_2$ layer was optimized by protein film voltammetry on FTO | IO-$TiO_2$ | $H_2$ase electrodes (FTO = fluorine-doped tin oxide; Figure S8). The performance of Si | IO-$TiO_2$ | $H_2$ase as a photocathode was studied by linear sweep voltammetry (LSV) under chopped, UV-, and IR-filtered simulated solar light irradiation (100 mW $cm^{-2}$; AM1.5G; $\lambda > 420$ nm; 25 °C). The electrolyte solution (pH 6.0) for LSV contained 50 mM MES (2-(*N*-morpholino)ethanesulfonic acid) and 50 mM KCl. A photocurrent onset potential was observed at approximately 0.35 V vs. the reversible hydrogen electrode (RHE), which is only slightly more positive than in $H_2$ase-free Si | IO-$TiO_2$ (Figures 2A and S9A). The photocurrent onset potential is therefore predominantly controlled by the Si-$TiO_2$ interface,[8] and the photocurrents on the short timescale of a voltammetric scan contain a significant contribution from the charging process of the $TiO_2$ conduction band. Charging of $TiO_2$ became evident from the large photocathodic

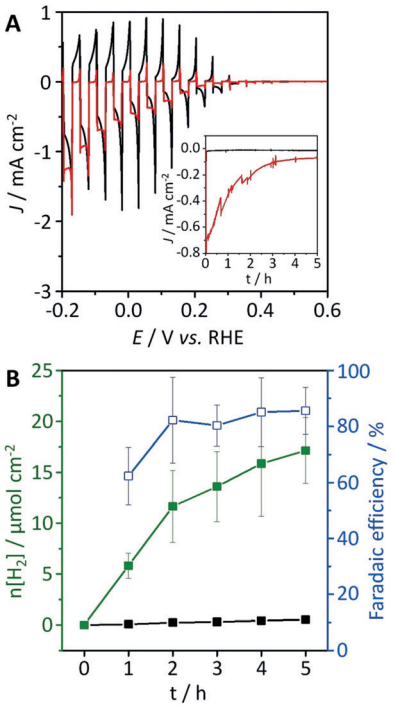


***Figure 2.*** A) LSV scans of Si | IO-$TiO_2$ (black) and Si | IO-$TiO_2$ | $H_2$ase (red) at a scan rate of 5 mV $s^{-1}$ under chopped-light irradiation (100 mW $cm^{-2}$; AM1.5G; IR water filter; $\lambda > 420$ nm; 25 °C). Inset: CPPE of the electrodes at 0.0 V vs. RHE. B) Time profiles of $H_2$ production (green) and the corresponding Faradaic efficiency (blue) during 5 h of CPPE at 0.0 V vs. RHE under visible-light irradiation for Si | IO-$TiO_2$ | $H_2$ase. The $H_2$ production for Si | IO-$TiO_2$ (black) is also shown for comparison (see also Figure S9C). Conditions: 50 mM of MES solution (pH 6.0) containing 50 mM KCl, $N_2$ atmosphere, room temperature, geometrical surface area: 0.178 $cm^2$ for all electrodes.

  

charging spikes and anodic current response in the dark phase of the light-chopped LSV scans. The ratio of the photocathodic to anodic charge is indeed close to unity for Si | IO-$TiO_2$, indicating negligible catalytic turnover. In contrast, the cathodic charge is far higher than the anodic response for $H_2$ase-modified electrodes, which supports efficient interfacial charge transfer and catalytic turnover at the enzyme.

Controlled potential photoelectrolysis (CPPE) with Si | IO-$TiO_2$ at 0.0 V vs. RHE showed a photocurrent close to zero after less than one minute (Figure 2A, inset; Figure S9B), and only a small amount of $H_2$ ($0.5 \pm 0.1$ μmol $cm^{-2}$) with a modest Faradaic efficiency ($45 \pm 9$%) was produced during 5 h (Figures 2B and S9C). In contrast, Si | IO-$TiO_2$ | $H_2$ase maintained good photocathodic currents during 5 h of CPPE (Figure 2A, inset), and headspace gas analysis by gas chromatography revealed the generation of $17 \pm 3$ μmol $cm^{-2}$ of $H_2$ with a Faradaic efficiency of ($86 \pm 8$)%. The $H_2$ase is therefore electroactive and relatively robust in the IO-$TiO_2$ scaffold. Control experiments in the presence of Pt nanoparticles instead of $H_2$ase showed comparable electrochemical responses (Figures S10 and S11).

The Si | IO-$TiO_2$ | $H_2$ase photocathode was then paired with photoanodes. Previously, the $H_2$ evolving *Clostridium acetobutylicum* [FeFe] hydrogenase HydA, adsorbed on a pyrolytic graphite edge electrode, had been connected to a porphyrin-sensitized $TiO_2$ photoanode. This PEC cell relied on the consumption of sacrificial NADH (nicotinamide adenine dinucleotide),[1d] whereas we demonstrate overall water splitting in this work. $BiVO_4$ is a well-established photoanode for water oxidation,[9] which was synthesized on FTO-coated glass according to previous reports.[10] $BiVO_4$ was selected owing to its stability under the neutral pH conditions required for the $H_2$ase, and its high photovoltage and currents are in principle suitable for bias-free water splitting when paired with a silicon photocathode.[9,10a,b] The synthesized $BiVO_4$ is crystalline and exhibits a film thickness of approximately 650 nm with a nanoporous surface structure (see Figure S12 for SEM images, XRD pattern, and UV/Vis spectrum). The kinetics of water oxidation was enhanced by deposition of a molecular TiCo precatalyst on the $BiVO_4$ surface from a single source precursor as previously reported.[10b,11]

FTO | $BiVO_4$ | TiCo exhibited a photocurrent of 1.0 mA $cm^{-2}$ at 1.23 V vs. RHE in MES/KCl solution (50 mM each, pH 6.0) for UV-filtered simulated solar light irradiation (100 mW $cm^{-2}$; AM1.5G; IR water filter; $\lambda > 420$ nm; 25 °C), driving water oxidation with high stability during the 5 h of CPPE (Figure S13). Comparison of the LSV scans of FTO | $BiVO_4$ | TiCo and Si | IO-$TiO_2$ | $H_2$ase obtained from three-electrode measurements showed a photocurrent of approximately 15 μA at the intersection of both voltammetric scans (0.18 V vs. RHE), suggesting the feasibility of unassisted water splitting in a tandem PEC cell (Figure 3A).

Thus a two-electrode configuration was adapted with a Nafion membrane separating the anodic from the cathodic compartment. Irradiation of the two-electrode tandem PEC cell without an external voltage ($U = 0$ V) for five hours gave a constant photocurrent profile and generated $0.47 \pm 0.09$ μmol of $H_2$ and 0.20 μmol of $O_2$, which corresponds to

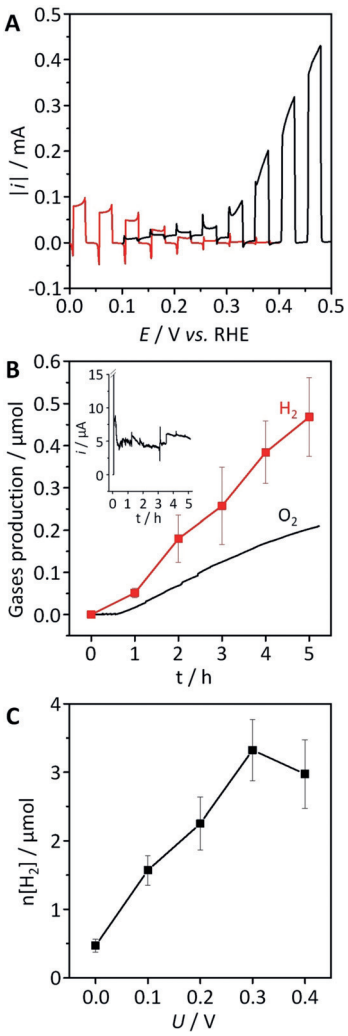


***Figure 3.*** A) LSV scans of FTO | $BiVO_4$ | TiCo (black) and Si | IO-$TiO_2$ | $H_2$ase (red) obtained from three-electrode measurements (note that the current for Si | IO-$TiO_2$ | $H_2$ase was inverted for ease of comparison). B) Time profiles of $H_2$ and $O_2$ production during unassisted solar water splitting in a two-electrode PEC cell with Si | IO-$TiO_2$ | $H_2$ase wired to FTO | $BiVO_4$ | TiCo in a two-electrode configuration. The inset shows the *I–t* trace from the CPPE measurement. C) Total amount of $H_2$ produced during 5 h PEC water splitting as a function of the applied voltage. In all experiments, the geometrical surface areas of FTO | $BiVO_4$ | TiCo and Si | IO-$TiO_2$ | $H_2$ase were 4 and 0.178 $cm^2$, respectively. Conditions: Visible-light irradiation (100 mW $cm^{-2}$; AM1.5G; IR water filter; $\lambda > 420$ nm; 25 °C), 50 mM of MES solution (pH 6.0) containing 50 mM KCl, $N_2$ atmosphere, room temperature.

Faradaic efficiencies of $98 \pm 14$% and 84%, respectively (Figure 3B). The performance of the tandem PEC cell was also studied with different external voltages (Figures 3C and S14). As expected, the photocurrent and the quantity of $H_2$ increased with higher voltages, maintaining a Faradaic efficiency of more than 80% after 5 h CPPE in all measurements.

The Si | IO-$TiO_2$ | $H_2$ase photocathode was subsequently paired with the biological water oxidation photocatalyst PSII (isolated from *Thermosynechococcus elongatus*) immobilized on an anode. $H_2$ase had previously been wired to PSII in

  

a PEC configuration, but both enzymes were immobilized on hierarchical IO-ITO electrodes.[3a] The single light-absorbing PEC cell contained a "dark" IO-ITO | $H_2$ase cathode, which resulted in the requirement of a large external voltage ($U >$ 0.6 V) to achieve overall water splitting. Our Si | IO-$TiO_2$ | $H_2$ase electrode provides a unique opportunity to reduce this thermodynamic barrier needed for overall water splitting using $H_2$ase and PSII.

The energetics of the electrons afforded by the IO-ITO | PSII anode is dependent on the terminal electron acceptors within PSII (quinones $Q_A$ and $Q_B$). To minimize energy loss of the electrons leaving PSII, a number of soluble $Q_B$ mimics with more negative redox potentials than the commonly employed mediator 2,6-dichloro-1,4-benzoquinone (DCBQ, $E_m = 329$ mV vs. NHE)[12] were studied. Although 2,6-di-*tert*-butyl-1,4-benzoquinone (DTBpQ, $E_m = 92$ mV vs. NHE) showed the most negative onset potential, it also exhibited low aqueous solubility, giving rise to lower overall photocurrents. As such, 3,5-di-*tert*-butyl-1,2-benzoquinone (DTBoQ, $E_m = 290$ mV vs. NHE) was identified as the most suitable redox shuttle to mediate charge at the PSII–ITO interface as it gives rise to a 100 mV earlier photocurrent onset than DCBQ (Figure S15). Comparing a stepped chronoamperometry scan of FTO | IO-ITO | PSII (90 pmol PSII; Figure S16) in the presence of DTBoQ with an LSV scan of Si | IO-$TiO_2$ | $H_2$ase shows that an applied voltage of $U >$ 0.24 V will be required for solar PEC water splitting (Figures 4 A and S17). A two-electrode PEC cell consisting of the FTO | IO-ITO | PSII photoanode coupled to the Si | IO-$TiO_2$ | $H_2$ase photocathode was irradiated with UV-filtered simulated solar light (100 mW cm$^{-2}$; AM1.5G; IR water filter; $\lambda > 420$ nm; 25 °C) for 3 h at $U = 0.4$ V, which resulted in the generation of $0.70 \pm 0.13$ μmol cm$^{-2}$ of $H_2$ with a Faradaic efficiency of $(91 \pm 19)$ % (Figure 4 B). This semi-artificial tandem PEC cell therefore allows for a wider usage of the solar spectrum at a reduced voltage than the previously reported[3a] single-light-absorber system.

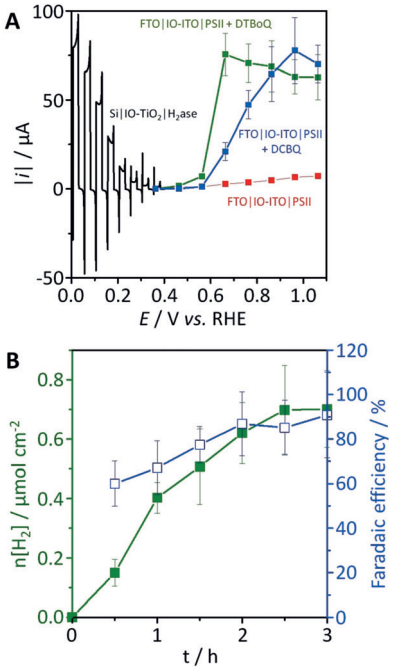


***Figure 4.*** A) Stepped chronoamperometry scans of FTO | IO-ITO | PSII without a soluble redox mediator (red), with DCBQ (blue), and with DTBoQ (green). An LSV scan of Si | IO-$TiO_2$ | $H_2$ase (black) with inverted current is also shown. The loading amounts of PSII and $H_2$ase were 90 and 80 pmol, respectively. All scans were carried out in a three-electrode configuration under chopped light irradiation. B) Time profiles of $H_2$ production (green) and the corresponding Faradaic efficiency (blue) during two-electrode PEC water splitting of FTO | IO-ITO | PSII with DTBoQ wired to Si | IO-$TiO_2$ | $H_2$ase at an applied voltage of 0.4 V. In all experiments, the geometrical surface areas of FTO | IO-ITO | PSII and Si | IO-$TiO_2$ | $H_2$ase were 0.5 and 0.178 cm$^2$, respectively. Conditions: Simulated solar light (100 mW cm$^{-2}$; AM1.5G; IR water filter; $\lambda > 420$ nm; 25 °C), 50 mM of MES solution (pH 6.0) containing 50 mM KCl, 1 mM of $Q_B$ mimics, $N_2$ atmosphere, room temperature.

In summary, we have developed a hierarchically structured photocathode and demonstrated by PEC, QCM, and ATR-IR analysis its excellent and stable integration of an electroactive $H_2$ase. This Si | IO-$TiO_2$ | $H_2$ase photocathode is a platform for the production of $H_2$ from tandem PEC water spitting with photoanodes. Using a $BiVO_4$ photoanode enabled stable and unassisted solar water splitting with a hydrogenase in vitro. Pairing of the $H_2$ase photocathode with a PSII photoanode allows tandem water splitting with wired enzymes in an engineered Z-scheme for complementary light absorption. The presented semi-artificial platform is suitable for the integration of a wide range of biological catalysts and guests in the future.

## Acknowledgements

This work was supported by an ERC Consolidator Grant "MatEnSAP" (D.H.N., J.Z.Z., N.H., E.R.), the University of Cambridge (Vice-Chancellor and Winton scholarships to V.A.), the Royal Society (Newton fellowship to N.K.), the Christian Doppler Research Association and OMV Group (A.W., E.R.), the EPSRC (Ph.D. studentship to K.P.S.; NanoDTC, EP/G037221/1, and EP/L015978/1 to K.N., S.H., and E.R.), the National Research Foundation of Korea (NRF-2015R1A3A2066191 to D.H.N., C.B.P.), and the German Research foundation (DFG) within the cluster of excellence EXC 314, "UniCat" (I.Z.). We thank Prof. A. William Rutherford and Dr Andrea Fantuzzi (Imperial College London) for providing a sample of PSII, Prof. Dominic S. Wright for the TiCo precatalyst, Marina Ianello and Dr Christine Cavazza for isolating and purifying the hydrogenase, and Dr. William E. Robinson for helpful discussions.

## Conflict of interest

The authors declare no conflict of interest.

**Keywords:** hydrogenase · photoelectrochemistry · photosynthesis · silicon · water splitting

  

**How to cite:** *Angew. Chem. Int. Ed.* **2018**, *57*, 10595 – 10599
*Angew. Chem.* **2018**, *130*, 10755 – 10759

[1] a) D. J. Evans, C. J. Pickett, *Chem. Soc. Rev.* **2003**, *32*, 268 – 275; b) C. Wombwell, C. A. Caputo, E. Reisner, *Acc. Chem. Res.* **2015**, *48*, 2858 – 2865; c) W. Lubitz, H. Ogata, O. Rüdiger, E. Reijerse, *Chem. Rev.* **2014**, *114*, 4081 – 4148; d) M. Hambourger, M. Gervaldo, D. Svedruzic, P. W. King, D. Gust, M. Ghirardi, A. L. Moore, T. A. Moore, *J. Am. Chem. Soc.* **2008**, *130*, 2015 – 2022.

[2] a) E. Reisner, D. J. Powell, C. Cavazza, J. C. Fontecilla-Camps, F. A. Armstrong, *J. Am. Chem. Soc.* **2009**, *131*, 18457 – 18466; b) C. A. Caputo, M. A. Gross, V. W. Lau, C. Cavazza, B. V. Lotsch, E. Reisner, *Angew. Chem. Int. Ed.* **2014**, *53*, 11538 – 11542; *Angew. Chem.* **2014**, *126*, 11722 – 11726; c) B. L. Greene, C. A. Joseph, M. J. Maroney, R. B. Dyer, *J. Am. Chem. Soc.* **2012**, *134*, 11108 – 11111; d) K. A. Brown, M. B. Wilker, M. Boehm, G. Dukovic, P. W. King, *J. Am. Chem. Soc.* **2012**, *134*, 5627 – 5636; e) G. A. M. Hutton, B. Reuillard, B. C. M. Martindale, C. A. Caputo, C. W. J. Lockwood, J. N. Butt, E. Reisner, *J. Am. Chem. Soc.* **2016**, *138*, 16722 – 16730; f) C. Tapia, S. Zacarias, I. A. C. Pereira, J. C. Conesa, M. Pita, A. L. De Lacey, *ACS Catal.* **2016**, *6*, 5691 – 5698; g) T. Sakai, D. Mersch, E. Reisner, *Angew. Chem. Int. Ed.* **2013**, *52*, 12313 – 12316; *Angew. Chem.* **2013**, *125*, 12539 – 12542.

[3] a) D. Mersch, C.-Y. Lee, J. Z. Zhang, K. Brinkert, J. C. Fontecilla-Camps, A. W. Rutherford, E. Reisner, *J. Am. Chem. Soc.* **2015**, *137*, 8541 – 8549; b) C. Tapia, R. D. Milton, G. Pankratova, S. D. Minteer, H.-E. Åkerlund, D. Leech, A. L. De Lacey, M. Pita, L. Gorton, *ChemElectroChem* **2017**, *4*, 90 – 95; c) Y. Zhao, N. C. Anderson, M. W. Ratzloff, D. W. Mulder, K. Zhu, J. A. Turner, N. R. Neale, P. W. King, H. M. Branz, *ACS Appl. Mater. Interfaces* **2016**, *8*, 14481 – 14487; d) L. Tian, B. Németh, G. Berggren, H. Tian, *J. Photochem. Photobiol. A* **2018**, https://doi.org/10.1016/j.jphotochem.2018.01.035.

[4] a) L. A. King, T. R. Hellstern, J. Park, R. Sinclair, T. F. Jaramillo, *ACS Appl. Mater. Interfaces* **2017**, *9*, 36792 – 36798; b) X. Qi, G. She, X. Huang, T. Zhang, H. Wang, L. Mu, W. Shi, *Nanoscale* **2014**, *6*, 3182 – 3189.

[5] a) C.-Y. Lee, H. S. Park, J. C. Fontecilla-Camps, E. Reisner, *Angew. Chem. Int. Ed.* **2016**, *55*, 5971 – 5974; *Angew. Chem.* **2016**, *128*, 6075 – 6078; b) J. J. Leung, J. Warnan, D. H. Nam, J. Z. Zhang, J. Willkomm, E. Reisner, *Chem. Sci.* **2017**, *8*, 5172 – 5180.

[6] a) A. Parkin, G. Goldet, C. Cavazza, J. C. Fontecilla-Camps, F. A. Armstrong, *J. Am. Chem. Soc.* **2008**, *130*, 13410 – 13416; b) E. Reisner, *Eur. J. Inorg. Chem.* **2011**, 1005 – 1016.

[7] A. Barth, *Biochim. Biophys. Acta Bioenerg.* **2007**, *1767*, 1073 – 1101.

[8] H. J. Kim, J. Seo, M. J. Rose, *ACS Appl. Mater. Interfaces* **2016**, *8*, 1061 – 1066.

[9] J. A. Seabold, K.-S. Choi, *J. Am. Chem. Soc.* **2012**, *134*, 2186 – 2192.

[10] a) Y. Kuang, Q. Jia, H. Nishiyama, T. Yamada, A. Kudo, K. Domen, *Adv. Energy Mater.* **2016**, *6*, 1501645; b) Y.-H. Lai, D. W. Palm, E. Reisner, *Adv. Energy Mater.* **2015**, *5*, 1501668; c) T. W. Kim, K.-S. Choi, *Science* **2014**, *343*, 990 – 994.

[11] a) Y.-H. Lai, C.-Y. Lin, Y. Lv, T. C. King, A. Steiner, N. M. Muresan, L. Gan, D. S. Wright, E. Reisner, *Chem. Commun.* **2013**, *49*, 4331 – 4333; b) Y.-H. Lai, T. C. King, D. S. Wright, E. Reisner, *Chem. Eur. J.* **2013**, *19*, 12943 – 12947.

[12] a) S. Lemieux, R. Carpentier, *J. Photochem. Photobiol. B* **1988**, *2*, 221 – 231; b) M. Kato, J. Z. Zhang, N. Paul, E. Reisner, *Chem. Soc. Rev.* **2014**, *43*, 6485 – 6497.

Manuscript received: April 30, 2018
Revised manuscript received: June 5, 2018
Accepted manuscript online: June 11, 2018
Version of record online: July 17, 2018

  